

# An Integral Line-of-Sight Guidance Law with a Speed-dependent Lookahead Distance

Martin S. Wiig<sup>1,2</sup>, Kristin Y. Pettersen<sup>1,2</sup>, Else-Line M. Ruud<sup>2</sup> and Thomas R. Krogstad<sup>2</sup>

**Abstract**—This paper presents an algorithm that makes an underactuated marine vehicle follow a straight line path while in the presence of a constant ocean current. When following the path, the vehicle maintains a desired surge speed which is measured relative to the water, and which may be constant or time-varying. The algorithm is an integral line-of-sight guidance law where the lookahead distance is designed to depend linearly on the desired relative surge speed of the vehicle. This dependency makes it possible to keep the maneuvering demands of the vehicle limited, even when the vehicle surge speed is large. It is shown that if the desired relative surge speed is constant along the path, the resulting error dynamics has a uniformly semiglobally exponentially stable equilibrium at the origin, thus achieving the path following and velocity control objectives. Furthermore, in the case of a general, time-varying desired speed trajectory, it is shown that the solutions of the system remain bounded. The results are supported by simulations, as well as experiments with an unmanned surface vehicle.

## I. INTRODUCTION

Precise path following is a requirement for several kinds of marine operations, such as sea bed surveying, underwater pipeline inspection and sub sea photography. To achieve such tasks, the vehicles will rely on a guidance system that steers the vehicle onto the path. These tasks can often be achieved by following a set of straight line segments. However, the desired speed along the path will vary. For example, during a transit task the vehicle may drive as fast as possible, while during a task involving underwater photography the speed needs to be quite low to avoid blurry images. Furthermore, many marine vehicles are underactuated and can be modeled as vehicles equipped with stern propellers and steering rudders only. This gives a control force in the forward direction (surge), and a control moment for orientation (yaw), but no sideways (sway) control force. In this paper we investigate a guidance law for straight-line path following for underactuated vehicles at varying desired forward speed.

Path following for underactuated marine vehicles has been considered for instance in [1]–[5]. The line-of-sight (LOS) family of guidance laws steers the vehicle towards a point on the path ahead of the it, and have proven well suited

for underactuated vehicles. The algorithm was presented [6], and it was shown in [7] that the algorithm provided uniform global  $\kappa$ -exponential stability (i.e. uniform global asymptotic stability (UGAS) and uniform local exponential stability (ULES) [8]) of the path error and the state errors of a simple vehicle model in 3 degrees of freedom (3-DOF). More complete models of the vehicles were analyzed in [9] and [10], while [11] proved uniform semiglobal exponential stability (USGES) of the LOS guidance.

Integral action was added in the integral line-of-sight (ILOS) guidance law in [12], where global stability was proved in the presence of a constant ocean current. By considering the vehicle velocity measured relative to the water, it was possible to extend this result to global  $\kappa$ -exponential stability in [13], and further to USGES in [14]. This is as close to uniform global exponential stability (UGES) which it is possible to get with LOS and ILOS guidance laws, as there is a trigonometric saturation in the kinematic representation.

An important design parameter for (I)LOS guidance laws is the lookahead distance  $\Delta$ . In [15], the speed dependency of the optimal lookahead distance for a given vessel employing the LOS guidance law was investigated. It was shown that the optimal  $\Delta$  increases with increasing surge speed of the vehicle. This matches with intuition, as a longer lookahead distance will give smoother turns at higher speed. In particular, it is to be expected that the overshoot of the system will be reduced, even in the presence of slow heading controllers. Furthermore, this also matches with how an experienced helmsman would steer a ship; the faster the ship goes, the further ahead the helmsman will look. Hence, in this paper, we propose a lookahead distance that increases linearly with the desired relative surge speed,  $u_{rd}$ .

Most of the previous work on (I)LOS guidance laws has assumed a constant  $u_{rd}$ . However, when the lookahead distance varies with  $u_{rd}$ , it is natural to investigate the case when  $u_{rd}$  is time-varying. Such a scenario occurs, for example, when an (I)LOS guidance law is combined with a desired surge speed trajectory to obtain trajectory tracking, as in [16] and [17], or formation control, as in [18]–[20].

In [16] and [17], a LOS guidance law is used to steer the vehicle heading, while a surge speed law is used to obtain trajectory following along the path. Straight-line paths and a constant lookahead distance are considered in [16], which proves that the system, including the dynamics, is  $\kappa$ -exponentially stable. More general curved paths, and a lookahead distance that varies with the desired trajectory following speed are considered in [17], which shows local

This work was partly supported by the Research Council of Norway through the Centres of Excellence funding scheme, project no. 223254 - NTNU AMOS

<sup>1</sup>Centre for Autonomous Marine Operations and Systems (NTNU AMOS), Department of Engineering Cybernetics, Norwegian University of Science and Technology, 7491 Trondheim, Norway. [Martin.Wiig@itk.ntnu.no](mailto:Martin.Wiig@itk.ntnu.no)

<sup>2</sup>Norwegian Defence Research Establishment (FFI), P.O. Box 25, N-2027 Kjeller, Norway.

exponential convergence for straight line paths, and ultimate boundedness for paths of limited curvature. In the latter paper, however, vehicle dynamics are not included.

In [18], a group of underactuated marine vehicles is kept in a formation following a straight line path. Each vehicle uses the LOS guidance law to converge to a desired offset of the path, while the desired surge speed trajectory makes the vehicles keep a desired relative along-track distance, while making the formation converge to a desired, constant along-track speed. Vehicle dynamics are considered, and it is proved that the vehicles converge to the formation exponentially.

When a vehicle follows a straight path using the ILOS guidance law in the presence of a constant ocean current, the vehicle heading will converge to a steady state value that exactly compensates for the current by making the vehicle side-slip along the path. However, if the vehicle speed changes along the path, the heading required to compensate for the current will not be constant, and there will not be an equilibrium point of the system unless the desired surge speed settles at a constant value. This is the case during the transient phase of the formation control algorithm presented in [19] and [20], where the vehicle heading is steered by the ILOS guidance law, and exponential convergence of the system was proved.

In this paper we consider a single vessel, with kinematics and dynamics modeled in 3-DOF. The vessel should follow a straight-line path in the presence of an ocean current that is uniform in time and space, and to this end we employ an ILOS guidance scheme. However, unlike the ILOS guidance presented in [12], we allow the lookahead distance to increase linearly with the desired surge speed  $u_{rd}$ , thus making the vehicle make slower, smoother turns at high speed, reducing overshoot. It is thus possible to make the vehicle converge to the desired path without overshoot for a broad range of values of  $u_{rd}$ , without having to tune the guidance law each time  $u_{rd}$  changes. For the special case when  $u_{rd}$  is constant, we show that the system is USGES. Furthermore, we show that the solutions of the system remain ultimately bounded when  $u_{rd}$  is time-varying. Unlike previous works, we do not look at a specific function for  $u_{rd}$ . Rather, we let  $u_{rd}$  be a general function, with no required bound on the size of the time derivative of  $u_{rd}$ . Thus, the result can be used for any desired surge trajectory, including but not limited to those used for trajectory tracking in [17] or formation control in [19].

This paper is organized as follows. Section II gives a mathematical description of the system involved, while the control system is presented in Section III and the resulting error dynamics derived in Section IV. In Section V we show that the system achieves USGES when  $u_{rd}$  is constant, while in Section VI we show that the solutions of the system are ultimately bounded when  $u_{rd}$  is time-varying. The guidance law is applied to a simulated underwater vehicle operation in the horizontal plane in Section VII, and experiments on an unmanned surface vehicle are described in Section VIII. Finally, some concluding remarks are given in Section IX.

## II. SYSTEM DESCRIPTION

### A. System Model

We use a 3-DOF model of the vehicle, where the position and orientation in an inertial frame  $i$  is contained in  $\mathbf{p} \triangleq [x, y, \psi]^T$ . The body-fixed velocity of the vessel is represented by  $\mathbf{v} \triangleq [u, v, r]^T$ , where  $u$  is the surge speed,  $v$  is the sway speed and  $r$  is the yaw rate.

We assume that the ocean current is bounded:

*Assumption 1:* The ocean current, represented as  $\mathbf{v}_c \triangleq [V_x, V_y, 0]^T$  in the  $i$  frame, is uniform in space and time and bounded by a constant  $V_{\max} \geq \|\mathbf{v}_c\|$ .

The current velocity in the body frame  $b$  is  $\mathbf{v}_c = \mathbf{R}^T(\psi)\mathbf{v}_c = [u_c, v_c, 0]^T$ , where  $\mathbf{R}(\psi)$  is the principal rotation matrix for a rotation by an angle  $\psi$  around the  $z$  axis. The body-fixed relative velocity is then given by  $\mathbf{v}_r \triangleq \mathbf{v} - \mathbf{v}_c = [u_r, v_r, r]^T$ , where  $u_r$  is the relative surge speed and  $v_r$  is the relative sway speed. We represent the vehicle in terms of these relative velocities as described in [21]:

$$\dot{\mathbf{p}} = \mathbf{R}(\psi)\mathbf{v}_r + \mathbf{v}_c, \quad (1a)$$

$$\mathbf{M}\dot{\mathbf{v}}_r + \mathbf{C}(\mathbf{v}_r)\mathbf{v}_r + \mathbf{D}\mathbf{v}_r = \mathbf{B}\mathbf{f}. \quad (1b)$$

Here,  $\mathbf{M} = \mathbf{M}^T > 0$  is the mass and inertia matrix including hydrodynamic added mass,  $\mathbf{C}$  is the Coriolis and centripetal matrix,  $\mathbf{D} > 0$  is the linear hydrodynamic damping matrix and  $\mathbf{B} \in \mathbb{R}^{3 \times 2}$  is the actuator configuration matrix. The control vector  $\mathbf{f} \triangleq [T_u, T_r]^T$  contains the surge thrust  $T_u$  and the rudder angle  $T_r$ .

The matrix  $\mathbf{C}$  is obtained from  $\mathbf{M}$  as described in [21], while the other system matrices can be expressed as:

$$\mathbf{M} \triangleq \begin{bmatrix} m_{11} & 0 & 0 \\ 0 & m_{22} & m_{23} \\ 0 & m_{23} & m_{33} \end{bmatrix}, \quad (2)$$

$$\mathbf{D} \triangleq \begin{bmatrix} d_{11} & 0 & 0 \\ 0 & d_{22} & d_{23} \\ 0 & d_{32} & d_{33} \end{bmatrix}, \mathbf{B} \triangleq \begin{bmatrix} b_{11} & 0 \\ 0 & b_{22} \\ 0 & b_{33} \end{bmatrix}. \quad (3)$$

To obtain these matrices we have assumed that the vehicle is port-starboard symmetric. Furthermore, we have assumed that the origin of frame  $b$  is located at a point  $(x_g^*, 0)$ , where  $x_g^*$  is the pivot point of the vehicle. The control input  $\tau_r$  is thus removed from the sway dynamics, i.e.  $\mathbf{M}^{-1}\mathbf{B}\mathbf{f} = [\tau_u, 0, \tau_r]^T$ , where  $\tau_u$  is the control force in surge and  $\tau_r$  is the control moment in yaw.

### B. System Model in Component Form

The vehicle model (1) can be represented in component form:

$$\dot{x} = u_r \cos(\psi) - v_r \sin(\psi) + V_x, \quad (4a)$$

$$\dot{y} = u_r \sin(\psi) + v_r \cos(\psi) + V_y, \quad (4b)$$

$$\dot{\psi} = r, \quad (4c)$$

$$\dot{u}_r = F_{u_r}(v_r, r) - \frac{d_{11}}{m_{11}}u_r + \tau_u, \quad (4d)$$

$$\dot{v}_r = X(u_r)r + Y(u_r)v_r, \quad (4e)$$

$$\dot{r} = F_r(u_r, v_r, r) + \tau_r. \quad (4f)$$

where the functions  $F_{u_r}(v_r, r)$ ,  $X(u_r)$ ,  $Y(u_r)$  and  $F_r(u_r, v_r, r)$  are defined in Appendix I.

### C. Desired surge speed

The desired surge speed,  $u_{rd}$ , can be time-varying, and satisfies the following assumptions:

*Assumption 2:* The desired surge speed is bounded by  $u_{rd} \in [u_{rd,m}, u_{rd,M}]$ , where  $u_{rd,m}$  and  $u_{rd,M}$  are positive constants and  $u_{rd,m} > V_{\max}$ .

*Assumption 3:* The time derivative of  $u_{rd}$ ,  $\dot{u}_{rd}$ , is piecewise continuous in  $t$  and bounded.

In order to analyze the effect of the time-varying part of  $u_{rd}$ , we divide  $u_{rd}$  into a constant and a time-varying component:

$$u_{rd}(t) = u_c + u_t(t), \quad (5)$$

such that  $\dot{u}_c = 0$  and  $\dot{u}_t = \dot{u}_{rd}$ .

The following assumption is made on  $Y(u_r)$ :

*Assumption 4:* The function  $Y(u_r)$  satisfies

$$Y(u_r) \leq -Y_{\min} < 0, \quad \forall u_r \in [u_{rd,m}, u_{rd,M}]. \quad (6)$$

*Remark 1:* The negativity of  $Y(u_r)$  is justified by noticing that  $Y(u_r) > 0$  would imply that the system is undamped or nominally unstable in sway, which is generally not the case by the mechanical design of the vehicle.

Furthermore, the function  $X(u_r)$  is a linear function in  $u_r$  as seen in (50), hence it is bounded by

$$|X(u_r)| \leq X_{\max}, \quad \forall u_r \in [u_{rd,m}, u_{rd,M}]. \quad (7)$$

### D. Control objective

The control objective is to make the vehicle modeled by (1) converge to a straight-line path in the presence of the unknown ocean current  $\mathbf{v}_c$ , while maintaining the desired relative surge speed  $u_{rd}(t)$ .

To simplify the analysis, and without any loss of generality, the inertial reference frame  $i$  is placed such that its  $x$ -axis is aligned with the desired path  $\mathcal{P}$ , such that  $\mathcal{P} \triangleq \{(x, y) \in \mathbb{R}^2 : y = 0\}$ . The objectives of the control system are then formalized as

$$\lim_{t \rightarrow \infty} y(t) = 0, \quad (8a)$$

$$\lim_{t \rightarrow \infty} u_r(t) = u_{rd}(t). \quad (8b)$$

## III. CONTROL SYSTEM

In this section we present an ILOS guidance scheme, along with the surge and yaw control laws, for solving the path following control problem presented in the previous section. The lookahead distance in the ILOS law is designed to increase linearly with the desired relative surge speed, in order to avoid sharp turns and oscillations at high speeds.

### A. The ILOS guidance law

The desired heading  $\psi_d$  is given by an ILOS guidance law:

$$\psi_d \triangleq -\tan^{-1}\left(\frac{y + \sigma y_{\text{int}}}{k_{\Delta} u_{rd}}\right), \quad k_{\Delta} > 0, \quad \sigma > 0, \quad (9a)$$

$$\dot{y}_{\text{int}} \triangleq \frac{k_{\Delta} u_{rd} y}{(y + \sigma y_{\text{int}})^2 + (k_{\Delta} u_{rd})^2}. \quad (9b)$$

The look-ahead gain  $k_{\Delta}$  and the integral gain  $\sigma$  are constant design parameters. The integral effect creates a nonzero desired heading even when the cross-track error  $y$  is zero, which compensates for the effect of the ocean current. The integral term growth rate (9b) decreases for large cross-track errors, reducing the risk of wind-up effects.

Unlike the guidance law presented in [12], this guidance law is designed to depend on the desired relative surge speed,  $u_{rd}$ , such that the lookahead distance is given as  $\Delta(u_{rd}) \triangleq k_{\Delta} u_{rd}$ . By looking farther ahead for large  $u_{rd}$ , the required maneuvering capabilities of the vehicle at high speed are reduced. Thus, the guidance law is designed to make the vehicle approach the path more gently, and to reduce the demands on the yaw controller and actuators.

*Remark 2:* We use the desired relative surge speed, rather than the measured relative surge speed, to decrease the coupling between the vehicle surge dynamics and the guidance law.

### B. Surge and yaw controllers

Surge and yaw are controlled using the feedback linearization controllers described in [22]:

$$\tau_u = -F_{u_r}(v_r, r) + \frac{d_{11}}{m_{11}} u_{rd} + \dot{u}_{rd} - k_{u_r}(u_r - u_{rd}), \quad (10)$$

$$\tau_r = -F_r(u_r, v_r, r) + \ddot{\psi}_d - k_{\psi}(\psi - \psi_d) - k_r(\dot{\psi} - \dot{\psi}_d), \quad (11)$$

where  $k_{u_r}$ ,  $k_{\psi}$  and  $k_r$  are constant, positive gains.

## IV. ERROR DYNAMICS

In this section we describe the error dynamics around the equilibrium point obtained when the desired surge speed is constant. For brevity, we will henceforth use the notation  $X^{u_{xx}} = X(u_{xx})$  and  $Y^{u_{xx}} = Y(u_{xx})$ .

### A. Actuated dynamics

The error signals of the actuated variables surge, yaw and yaw rate are collected in  $\zeta \triangleq [\tilde{u}_r, \tilde{\psi}, \dot{\tilde{\psi}}]^T$ , where  $\tilde{u}_r \triangleq u_r - u_{rd}$ ,  $\tilde{\psi} = \psi - \psi_d$  and  $\dot{\tilde{\psi}} \triangleq \dot{\psi} - \dot{\psi}_d$ . When the control laws in surge (10) and yaw (11) are applied to the system (4c), (4d) and (4f), the error dynamics of  $\zeta$  becomes:

$$\dot{\zeta} = \begin{bmatrix} -k_{u_r} - \frac{d_{11}}{m_{11}} & 0 & 0 \\ 0 & 0 & 1 \\ 0 & -k_{\psi} & -k_r \end{bmatrix} \zeta \triangleq \Sigma \zeta. \quad (12)$$

Since the term  $d_{11}/m_{11}$  and the gains  $k_{u_r}$ ,  $k_{\psi}$  and  $k_r$  are all strictly positive,  $\Sigma$  is Hurwitz and the origin,  $\zeta = \mathbf{0}$ , is UGES.

## B. Underactuated dynamics

The underactuated  $y-v_r$  dynamics are obtained from (4b), (4e) and (9b):

$$\dot{y}_{\text{int}} = \frac{k_{\Delta} u_{rd} y}{(y + \sigma y_{\text{int}})^2 + (k_{\Delta} u_{rd})^2}, \quad (13a)$$

$$\dot{y} = u_r \sin(\tilde{\psi} + \psi_d) + v_r \cos(\tilde{\psi} + \psi_d) + V_y, \quad (13b)$$

$$\dot{v}_r = X(\tilde{u}_r + u_{rd})(\dot{\tilde{\psi}} + \dot{\psi}_d) + Y(\tilde{u}_r + u_{rd})v_r. \quad (13c)$$

The heading required to compensate for the current varies with  $u_{rd}$ . Hence, there is no equilibrium point of (13) when  $\dot{u}_{rd} \neq 0$ . However, in the case when  $u_{rd}$  is constant for each line segment, that is when  $u_{rd} = u_c$ , then the equilibrium point of (13) on the manifold  $\zeta = \mathbf{0}$  is given by

$$y_{\text{int}}^{\text{eq}} = \frac{k_{\Delta}}{\sigma} \frac{V_y}{\sqrt{1 - \frac{V_y^2}{u_c^2}}}, \quad y^{\text{eq}} = 0, \quad v_r^{\text{eq}} = 0. \quad (14)$$

The error dynamics around this point is obtained by performing a change of variables:

$$e_1 \triangleq y_{\text{int}} - y_{\text{int}}^{\text{eq}}, \quad e_2 \triangleq y + \sigma e_1, \quad e_3 \triangleq v_r. \quad (15)$$

Factorizing with respect to  $\zeta$ , allows us to express the interconnected dynamics of (12) and (13) in cascaded form:

$$\dot{e} = \mathbf{A}(e_2)e + \mathbf{B}(e_2) + \mathbf{G}(e_2) + \mathbf{H}(e_2, e_3, \psi_d, \zeta)\zeta, \quad (16a)$$

$$\dot{\zeta} = \Sigma\zeta, \quad (16b)$$

where  $e \triangleq [e_1, e_2, e_3]^T$ ,  $\mathbf{A}$  is given in (18) while

$$\mathbf{B} \triangleq \begin{bmatrix} 0 \\ V_y f(e_2) \\ -\frac{k_{\Delta} u_{rd} X^{u_{rd}} V_y}{h(e_2)} f(e_2) \end{bmatrix}. \quad (17)$$

The function  $h(e_2)$  is defined as

$$h(e_2) \triangleq (e_2 + \sigma y_{\text{int}}^{\text{eq}})^2 + (k_{\Delta} u_{rd})^2, \quad (19)$$

and  $f(e_2)$  is defined as

$$f(e_2) \triangleq 1 - \frac{\sqrt{(\sigma y_{\text{int}}^{\text{eq}})^2 + (k_{\Delta} u_{rd})^2}}{\sqrt{h(e_2)}}. \quad (20)$$

Note that  $f(e_2)$  is bounded by:

$$|f(e_2)| \leq \frac{|e_2|}{\sqrt{h(e_2)}}. \quad (21)$$

The terms that vanish when  $\zeta = 0$  are collected in  $\mathbf{H}$ :

$$\mathbf{H} \triangleq \begin{bmatrix} 0 & 0 \\ 1 & 0 \\ -\frac{k_{\Delta} u_{rd} X(\tilde{u}_r + u_{rd})}{h(e_2)} & 1 \end{bmatrix} \begin{bmatrix} \mathbf{h}_{e_2}^T \\ \mathbf{h}_{e_3}^T \end{bmatrix}, \quad (22)$$

where  $\mathbf{h}_{e_2}$  and  $\mathbf{h}_{e_3}$  are given in Appendix I. The vector  $\mathbf{G}$  contains the terms that vanish when  $\dot{u}_{rd} = \dot{u}_t = 0$  and, by (5),  $u_t = 0$ :

$$\mathbf{G} \triangleq \begin{bmatrix} 0 \\ -\frac{\sigma y_{\text{int}}^{\text{eq}}}{\sqrt{h(e_2)}} u_t \\ \frac{X^{u_{rd}} k_{\Delta}}{h(e_2)} \left[ \left( \frac{\rho}{\sqrt{h(e_2)}} - V_y \right) u_t + (\sigma y_{\text{int}}^{\text{eq}} + e_2) \dot{u}_{rd} \right] \end{bmatrix}, \quad (23)$$

where  $\rho = (u_t + 2u_c)\sigma y_{\text{int}}^{\text{eq}}$ .

## V. CONSTANT DESIRED SURGE SPEED

This section analyzes the stability properties of the system when  $u_{rd}$  is constant, which means that  $u_{rd} = u_c$ ,  $u_t = 0$  and  $\dot{u}_{rd} = 0$ . We use the analysis to find analytical bounds on the ILOS parameters  $k_{\Delta}$  and  $\sigma$ , ensuring USGES of the equilibrium point of the closed-loop error dynamics.

### A. Stability of the nominal system

When  $\dot{u}_{rd} = u_t = 0$  we have that  $\mathbf{G} = 0$  as seen from (23). The nominal system of the cascade in (16) is then given by

$$\dot{e} = \mathbf{A}(e_2)e + \mathbf{B}(e_2). \quad (24)$$

*Lemma 1:* If Assumptions 1 to 2 hold,  $\dot{u}_{rd} = 0$ , and the look-ahead distance gain  $k_{\Delta}$  and the integral gain  $\sigma$  satisfy

$$k_{\Delta} > \frac{|X_{\text{max}}|}{|Y_{\text{min}}| u_{rd,m}} \left[ \frac{5 u_{rd,M} + V_{\text{max}} + \sigma}{4 u_{rd,m} - V_{\text{max}} - \sigma} + 1 \right], \quad (25)$$

$$0 < \sigma < u_{rd,m} - V_{\text{max}}, \quad (26)$$

then the equilibrium point of (24) is USGES.

*Proof:* The proof follows along the lines of [14], [22], while making use of the results in [23] to prove USGES.

Consider the Lyapunov function candidate (LFC):

$$V \triangleq \frac{1}{2} \sigma^2 e_1^2 + \frac{1}{2} e_2^2 + \frac{1}{2} \mu e_3^2, \quad \mu > 0. \quad (27)$$

Using Assumption 1 to 4, and equations (7) and (21), the following bound can be found for  $\dot{V}$ :

$$\dot{V} \leq -\frac{1}{h(e_2)} (L_1(e_{13}) + L_2(e_{23})), \quad (28)$$

where  $e_{13} \triangleq [|e_1|, |e_3|]^T$  and  $e_{23} \triangleq [|e_2|, |e_3|]^T$ .  $L_1$  is

$$L_1 \triangleq e_{13}^T \mathbf{Q}_1 e_{13}, \quad (29)$$

where  $\mathbf{Q}_1$  is

$$\mathbf{Q}_1 \triangleq \begin{bmatrix} k_{\Delta} \sigma^3 u_{rd,m} & -\frac{1}{2} \frac{\mu \sigma^2 \sqrt{h(e_2)} |X_{\text{max}}|}{k_{\Delta} u_{rd,m}} \\ -\frac{1}{2} \frac{\mu \sigma^2 \sqrt{h(e_2)} |X_{\text{max}}|}{k_{\Delta} u_{rd,m}} & \mu \eta h(e_2) \left( |Y_{\text{min}}| - \frac{|X_{\text{max}}|}{k_{\Delta} u_{rd,m}} \right) \end{bmatrix} \quad (30)$$

and  $0 < \eta < 1$ .  $L_2$  is defined as

$$L_2 \triangleq k_{\Delta} u_{rd,m} e_{23}^T \mathbf{Q}_2 e_{23}, \quad (31)$$

where  $\mathbf{Q}_2$  is

$$\mathbf{Q}_2 \triangleq \begin{bmatrix} \beta & -\alpha \sqrt{h(e_2)} \\ -\alpha \sqrt{h(e_2)} & h(e_2) \frac{\alpha(2\alpha-1)}{\beta} \end{bmatrix}. \quad (32)$$

Here,  $\beta \triangleq u_{rd,m} - V_{\text{max}} - \sigma$  and  $\alpha$  is given by

$$\alpha \triangleq (1-\eta) \frac{(u_{rd,m} - V_{\text{max}} - \sigma)(k_{\Delta} u_{rd,m} |Y_{\text{min}}| - |X_{\text{max}}|)}{|X_{\text{max}}|(u_{rd,M} + V_{\text{max}} + \sigma)}. \quad (33)$$

The parameter  $\mu$  is chosen as

$$\mu \triangleq \frac{(k_{\Delta} u_{rd,m})^2 (2\alpha - 1)}{|X_{\text{max}}|(u_{rd,M} + V_{\text{max}} + \sigma)}. \quad (34)$$

$$\mathbf{A} \triangleq \begin{bmatrix} -\frac{\sigma k_\Delta u_{rd}}{h(e_2)} & \frac{k_\Delta u_{rd}}{h(e_2)} & 0 \\ -\frac{\sigma^2 k_\Delta u_{rd}^2}{h(e_2)} & \frac{\sigma k_\Delta u_{rd}}{h(e_2)} - \frac{u_{rd}}{\sqrt{h(e_2)}} & \frac{k_\Delta u_{rd}}{\sqrt{h(e_2)}} \\ \frac{\sigma^2 k_\Delta^2 u_{rd}^2 X^{urd}}{h(e_2)^2} & \left( \frac{k_\Delta u_{rd}^2 X^{urd}}{h(e_2)^{3/2}} - \frac{\sigma k_\Delta^2 u_{rd}^2 X^{urd}}{h(e_2)^2} \right) & \left( Y^{urd} - \frac{k_\Delta^2 u_{rd}^2 X^{urd}}{h(e_2)^{3/2}} \right) \end{bmatrix} \quad (18)$$

If  $\mathbf{Q}_1$  and  $\mathbf{Q}_2$  are positive definite, then  $\dot{V}$  is negative definite. Positive definiteness of  $\mathbf{Q}_1$  is ensured when

$$k_\Delta > \frac{|X_{\max}|}{|Y_{\min}| u_{rd,m}}, \quad (35)$$

$$\mu < \frac{4\eta k_\Delta^2 u_{rd,m} (k_\Delta u_{rd,m} |Y_{\min}| - |X_{\max}|)}{\sigma |X_{\max}|^2}. \quad (36)$$

Condition (35) is met as long as (25) holds. It can be shown that  $\eta \geq 1/5$  is a sufficient condition for  $\mu$  to satisfy (36). Thus, without loss of generality,  $\eta$  is set to  $1/5$ , and positive definiteness of  $\mathbf{Q}_1$  is ensured.

Positive definiteness of  $\mathbf{Q}_2$  is ensured if  $\beta > 0$  and  $\alpha > 1$ . Assumption 2 and (26) ensure that  $\beta > 0$ , while conditions (25) and (26) ensure that  $\alpha > 1$ .

Let  $\mathbf{Q}$  be the symmetric  $3 \times 3$  matrix defined from  $L_1(\mathbf{e}_{13})$  and  $L_2(\mathbf{e}_{23})$  so that

$$\mathbf{e}^T \mathbf{Q} \mathbf{e} = L_1(\mathbf{e}_{13}) + L_2(\mathbf{e}_{23}). \quad (37)$$

Since both  $\mathbf{Q}_1$  and  $\mathbf{Q}_2$  are positive definite, so is  $\mathbf{Q}$ . Hence, the following bound holds:

$$\dot{V} \leq -\frac{1}{h(e_2)} q_{\min} \|\mathbf{e}\|^2, \quad (38)$$

where  $q_{\min} \triangleq \lambda_{\min}(\mathbf{Q})$ , the minimum eigenvalue of  $\mathbf{Q}$ . In any ball  $\mathcal{B}_r \triangleq \{|e_2| < r\}$ ,  $r > 0$  the function  $h(e_2)$  is upper bounded as

$$h(e_2) \leq (r + \sigma y_{\text{int}}^{\text{eq}})^2 + (k_\Delta u_{rd})^2 := c(r). \quad (39)$$

Hence, for any  $r > 0$

$$\dot{V} \leq -\frac{q_{\min}}{c(r)} \|\mathbf{e}\|^2 \quad (40)$$

Thus, the conditions of [23, Theorem 5] is fulfilled with  $k_1 = \frac{1}{2} \min\{\sigma^2, 1, \mu\}$ ,  $k_2 = \frac{1}{2} \max\{\sigma^2, 1, \mu\}$  and  $k_3 = \frac{q_{\min}}{c(r)}$ . Hence, the equilibrium point  $\mathbf{e} = \mathbf{0}$  is USGES as defined in [23, Definition 1]. ■

### B. Stability property of the closed-loop system

*Theorem 1:* If Assumptions 1 to 2 hold,  $\dot{u}_{rd} = 0$ , and the look-ahead distance gain  $k_\Delta$  and the integral gain  $\sigma$  satisfy

$$k_\Delta > \frac{|X_{\max}|}{|Y_{\min}| u_{rd,m}} \left[ \frac{5 u_{rd,m} + V_{\max} + \sigma}{4 u_{rd,m} - V_{\max} - \sigma} + 1 \right], \quad (41)$$

$$0 < \sigma < u_{rd,m} - V_{\max}, \quad (42)$$

then the controllers (10) and (11), where  $\psi_d$  is given by (9), guarantee achievement of the control objectives (8). Furthermore, the equilibrium point of the error dynamics (16) is USGES and UGAS.

*Proof:* The system (16) is a cascaded system, where (16b) perturbs the dynamics (16a) through the interconnection matrix  $\mathbf{H}$ . The interconnection matrix  $\mathbf{H}$  can be shown

to satisfy  $\|\mathbf{H}\| \leq \theta_1(\|\boldsymbol{\zeta}\|)(|y| + |y_{\text{int}}| + |v_r|) + \theta_2(\|\boldsymbol{\zeta}\|)$ , where  $\theta_1(\cdot)$  and  $\theta_2(\cdot)$  are some continuous non-negative functions. The perturbing system is UGES as shown in Section IV-A, and the nominal system is USGES by Lemma 1. Hence all the conditions of [24, Proposition 2.3] are satisfied, guaranteeing USGES and UGAS of the origin of (16). ■

## VI. TIME-VARYING DESIRED SURGE SPEED

In this section we allow  $u_{rd}$  to vary with time:  $\dot{u}_{rd} \neq 0$  and  $u_t \neq 0$ . As noted in Section IV-B, there is no equilibrium point of the system in this case. However, inspired by the approach in [19], we will treat the time-varying  $u_t$  component of  $u_{rd}$  as a disturbance. It can then be proved that the solutions of the system remain bounded around the equilibrium point obtained in (14). To this end we will apply Lemma 12 from [23].

In this section, we will use the constants  $k_1 \triangleq \frac{1}{2} \min\{\sigma^2, 1, \mu\}$ ,  $k_2 \triangleq \frac{1}{2} \max\{\sigma^2, 1, \mu\}$ ,  $k_3 \triangleq \frac{q_{\min}}{c(r)}$  and  $k_4 \triangleq 2k_2$ , where  $k_1$  to  $k_3$  are obtained from the proof of Lemma 1.

### A. Boundedness of the nominal system

Since  $\dot{u}_{rd} \neq 0$ , the nominal system of the cascade (16) becomes:

$$\dot{\mathbf{e}} = \mathbf{A}(e_2)\mathbf{e} + \mathbf{B}(e_2) + \mathbf{G}(e_2). \quad (43)$$

*Lemma 2:* Assume that the conditions of Theorem 1 are satisfied, with the exception that  $\dot{u}_{rd} \neq 0$ . Then there exists a positive constant  $\delta$ , a constant  $c \in (0, 1)$  and a time  $T \geq 0$ , such that the solutions of (43) satisfy

$$\|\mathbf{e}(t)\| \leq \sqrt{\frac{k_2}{k_1}} \|\mathbf{e}(t_0)\| e^{-\frac{(1-c)k_3}{2+k_2}(t-t_0)} \quad (44)$$

$\forall t_0 \leq t \leq t_0 + T$ , and

$$\|\mathbf{e}(t)\| \leq \frac{k_4}{k_3} \sqrt{\frac{k_2}{k_1}} \frac{\delta}{c} \quad \forall t \geq t_0 + T. \quad (45)$$

*Proof:* The partial derivative of (27) is bounded by

$$\left\| \frac{\partial V}{\partial \mathbf{e}} \right\| \leq \max\{\sigma^2, 1, \mu\} \|\mathbf{e}\|. \quad (46)$$

Hence, condition (32) of [23, Lemma 12] is satisfied with  $k_4 = \max\{\sigma^2, 1, \mu\} = 2k_2$  and  $a = 2$ . It remains to show that  $\|\mathbf{G}\|$  is bounded for large  $\|\mathbf{e}\|$ . We do this by noticing that the denominators in  $\mathbf{G}$  are strictly positive functions of higher order of  $e_2$  than the numerators. Hence, it is always possible to choose an  $\bar{r} > 0$  large enough so that in a ball  $\mathcal{B}_{\bar{r}} \triangleq \{|e_2| < \bar{r}\}$ , we have that

$$\|\mathbf{G}\| \leq \delta < \frac{k_3}{k_4} \sqrt{\frac{k_1}{k_2}} \bar{r} c, \quad (47)$$

for some  $\delta > 0$  and  $c \in (0, 1)$ . Hence, the conditions of [23, Lemma 12] are satisfied, and the solutions of (43) are uniformly globally bounded by (44) and (45). ■

Notice that the solutions of (45) are bounded regardless of the maximum magnitude of  $\dot{u}_{rd}$ .

### B. Boundedness of the complete system

Finally, we will show that the complete cascade (16) is uniformly bounded as well.

*Theorem 2:* Assume that the conditions of Theorem 1 are satisfied, with the exception that  $\dot{u}_{rd} \neq 0$ . Then the solutions of the cascaded system (16) are uniformly bounded.

*Proof:* We define the constant  $\bar{\delta}$  as the bound on  $\|e(t)\|$  in (45):

$$\bar{\delta} \triangleq \frac{k_4}{k_3} \sqrt{\frac{k_2}{k_1}} \frac{\delta}{c}. \quad (48)$$

It follows from (44) that the ball  $\mathcal{B}_{\bar{\delta}}$  is UGAS. Furthermore, the interconnection matrix  $\mathbf{H}$  can be shown to satisfy  $\|\mathbf{H}\| \leq \theta_3(\|\zeta\|)(|y| + |y_{\text{int}}| + |v_r|) + \theta_4(\|\zeta\|)$ , where  $\theta_3(\cdot)$  and  $\theta_4(\cdot)$  are some continuous non-negative functions. The perturbing system (16b) is UGES as shown in Section IV-A. Hence all the conditions of [24, Proposition 2.3] are satisfied, which implies that the set  $\mathcal{B}_{\bar{\delta}} \cup \{0\}$  is UGAS. This also implies that the solutions of the complete cascade (16) are uniformly globally bounded, which concludes the proof. ■

## VII. SIMULATIONS

In this section we present the results from numerical simulations of a system where the ILOS guidance law with speed-dependent lookahead distance (9) is applied to an underactuated AUV operating in the horizontal plane. The path is aligned with the  $x$  axis, and the AUV is modeled in 3-DOF as in (1).

The desired relative surge speeds are in the range  $u_{rd} \in [1.5, 2.5]$  m/s. The current is set to  $\mathbf{v}_c = [0 \text{ m/s}, 0.4 \text{ m/s}, 0 \text{ rad/s}]$ , which fulfills Assumption 1 and 2. It can be verified that Assumption 4 is satisfied with  $Y_{\min} = 1.01 \text{ s}^{-1}$ , and that  $X_{\max} = 1.84 \text{ s}^{-1}$ . The integral gain is  $\sigma = 0.3 \text{ m/s}$ , which satisfies (42). From these parameters, a lower limit on  $k_{\Delta}$  is found from (41) as  $k_{\Delta} = 7.34 \text{ s}$ . The surge controller gain is set to  $k_{u_r} = 0.5$ , while the heading controller gains are  $k_{\psi} = 0.025$  and  $k_r = 0.1$ . Thus, the yaw dynamics of the vehicle are quite slow, to simulate the effect of low-speed actuators.

In the first simulation scenario, we look at the effect of increasing  $k_{\Delta}$ . The desired relative surge speed is kept constant at  $u_{rd} = 2.5 \text{ m/s}$ , while  $k_{\Delta}$  goes from 8 s to 14 s in steps of 2 s. The initial position of the vehicle is 50 m away from the path, pointing straight towards the path with the initial relative surge speed set to  $u_r = u_{rd}$ . The cross track error for the different values of  $k_{\Delta}$  are shown in Figure 1. It can be seen that for lower values of  $k_{\Delta}$  there is an overshoot, which disappears for  $k_{\Delta} = 12 \text{ s}$ . The system remains stable for all values of  $k_{\Delta}$ , though, which verifies Theorem 1.

In the next simulation we use a fixed  $k_{\Delta} = 12 \text{ s}$ , but vary the desired relative surge speed from 1.5 m/s to 2.5 m/s in steps of 0.5 m/s. For each run, the vehicle initial position is

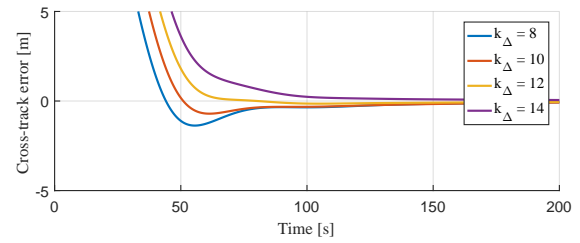


Fig. 1. The cross-track error  $y$  for increasing values of  $k_{\Delta}$  with  $u_{rd} = 2.5 \text{ m/s}$ .

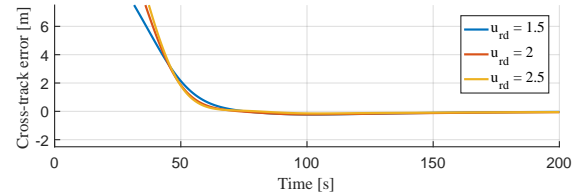


Fig. 2. The cross-track error  $y$  for increasing values of  $u_{rd}$  with  $k_{\Delta} = 12 \text{ s}$

set to  $20u_{rd}$  m away from the path, with the initial relative surge speed set to  $u_r = u_{rd}$ . Thus, the vehicle will use approximately the same amount of time to reach the path, making the results easier to compare. The cross track error of the three runs are displayed in Figure 2, and it can be seen that in each case the vehicle converges to the path without any overshoot.

Figure 3 shows the result from a scenario where the lookahead distance was kept constant at  $k_{\Delta}u_{rd} = 30 \text{ m}$ . It can be seen that the convergence times when  $u_{rd} = 2.0 \text{ m}$  and  $u_{rd} = 1.5 \text{ m}$  are significantly slower compared to the convergence times in Figure 2.

In the last scenario, we simulate a case with time-varying  $u_{rd}$ . Here  $u_{rd} = u_c + u_t$ , where  $u_c = 2.0 \text{ m/s}$  and  $u_t$  is a sine wave with amplitude 0.5 m and period 60 s. From Figure 4, it is clear that the cross-track error converges to a bounded set around  $y = 0$ . Thus, the simulation verifies Lemma 2 for this particular case.

## VIII. EXPERIMENTAL RESULTS

In this section we present the results from experiments at sea. The experiments were carried out on the Odin unmanned surface vehicle (USV), which is depicted in Figure 5. The vehicle developed by FFI and Kongsberg Maritime, is

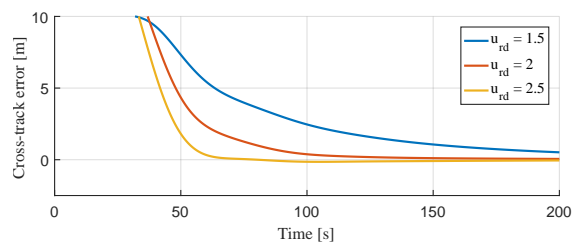


Fig. 3. The cross-track error  $y$  for increasing values of  $u_{rd}$  with constant lookahead distance  $\Delta = 30 \text{ m}$

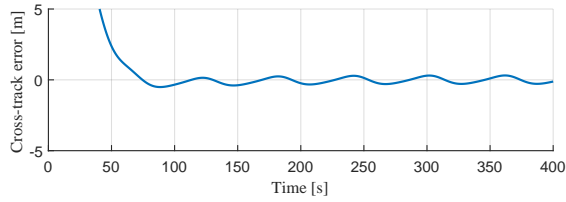


Fig. 4. The cross-track error  $y$  for a time-varying  $u_{rd}$ .



Fig. 5. The Odin USV

11 m long and 3.5 m wide, and is propelled by a dual waterjet system. At maneuvering speeds, the vehicle is underactuated. The ILOS guidance law was implemented with  $k_{\Delta}$  varying from 6 s to 12 s, and integral gain  $\sigma = 0.02$  m/s. The vehicle heading is controlled by a PD controller, which has been tuned to provide asymptotic stability of the heading.

The USV was tasked to follow a square pattern at different forward velocities. The waypoint switching distance was set to  $9u_{rd}$  m. Thus, the initial conditions for each line was similar to the initial conditions used in the simulations in Section VII, with the vehicle approaching the line at a perpendicular angle with initial offset increasing with desired surge speed.

Figure 7 displays the cross-track error for two lines with  $u_{rd} = 6$  m/s and  $k_{\Delta} = 6$  s and 12 s. In both cases, the cross-track error converges towards zero, however the overshoot is slightly larger for  $k_{\Delta} = 6$  s.

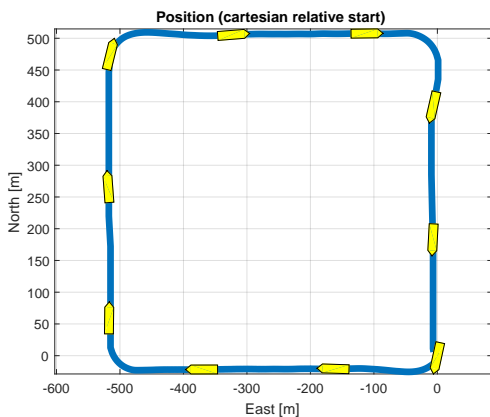


Fig. 6. The vehicle position relative to the starting position during a run with  $u_{rd} = 6$  m/s. The size of the vehicle has been increased in the figure.

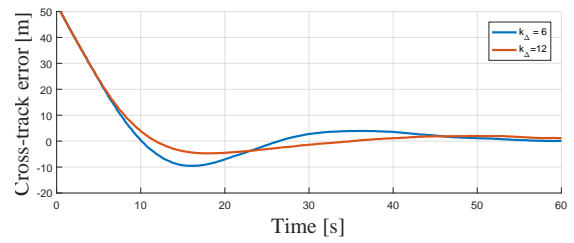


Fig. 7. The cross-track error for  $k_{\Delta} = 6$  s and 12 s with  $u_{rd} = 2.5$  m/s.

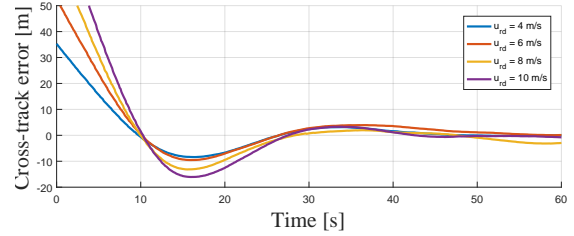


Fig. 8. The cross-track error for increasing values of  $u_{rd}$  with  $k_{\Delta} = 6$  s

Figure 8 shows the cross-track error during four lines with  $u_{rd}$  increasing from 4 m/s to 10 m/s with a lookahead gain of  $k_{\Delta} = 6$  s. In each case, the cross-track error reaches 0 m after approximately 11 s. We see that the overshoot increases slightly with increasing speed. A larger value of  $k_{\Delta}$  would likely decrease this effect, as would a larger switching distance between waypoints.

## IX. CONCLUSIONS

In this paper we have investigated an ILOS guidance law where the lookahead distance increases linearly with the desired surge speed  $u_{rd}$ . The work is motivated by the need to keep the maneuvering demands on a vehicle within acceptable limits, even when the surge speed is large. This is of particular importance if the dynamics of the vehicle yaw controller and actuators are slow with respect to the surge speed, in which case a small lookahead distance can lead to significant overshoot and oscillatory behavior.

Both the case when  $u_{rd}$  is constant along the path and the case where  $u_{rd}$  is time-varying have been explored. For a constant  $u_{rd}$ , we derive a lower bound on the lookahead gain and an upper bound on the ILOS integral gain in order to guarantee USGES of the system. In the case of a time-varying  $u_{rd}$ , we have proved that the solutions of the system remain bounded for bounded  $u_{rd}$ . This holds for general  $u_{rd}$  trajectories, with the only assumption that it is lower bounded above the level of the maximum ocean current, so that the vehicle is able to move forward also when it is heading directly against the ocean currents.

The stability and boundedness results have been verified in simulations of an underwater vehicle with slow yaw dynamics, moving in the horizontal plane. In particular, the simulations show how a lookahead distance that is linearly increasing with  $u_{rd}$  results in convergence to the desired path without overshoot for several values of  $u_{rd}$ . This is achieved without having to tune the guidance law each time  $u_{rd}$

changes. A simulation with a time-varying  $u_{rd}$  has also been presented, demonstrating that the cross-track error remains bounded in this case.

The ILOS guidance law with speed-dependent lookahead distance has also been implemented on the Odin USV, which has been used for experimental verification of the stability properties. We show that by increasing the lookahead distance linearly with  $u_{rd}$  the increase in overshoot at higher speeds are limited, and that the vehicle converges to the path for high and low values of  $u_{rd}$ .

### ACKNOWLEDGMENT

The authors would like to thank Jarle Sandrib at FFI for his valuable help and assistance during the experiments with the Odin USV.

### REFERENCES

- [1] P. Encarnação, A. Pascoal, and M. Arcac, "Path Following for Autonomous Marine," in *Proc. 5th IFAC Conference on Manoeuvring and Control of Marine Craft*, (Aalborg, Denmark), pp. 117–122, 2000.
- [2] G. Indiveri, M. Pino, M. Aicardi, and G. Casalino, "Nonlinear Time-Invariant Feedback Control of An Underactuated Marine Vehicle Along A Straight Course," in *Proc. 5th IFAC Conference on Manoeuvring and Control of Marine Craft*, (Aalborg, Denmark), pp. 221–226, 2000.
- [3] L. Lapiere, D. Soetanto, and A. Pascoal, "Nonlinear path following with applications to the control of autonomous underwater vehicles," in *Proc. 42nd IEEE Conference on Decision and Control (CDC)*, vol. 2, (Maui, HI, USA), pp. 1256–1261, 2003.
- [4] K. D. Do, Z. P. Jiang, and J. Pan, "Underactuated ship global tracking under relaxed conditions," *IEEE Transactions on Automatic Control*, vol. 47, no. 9, pp. 1529–1536, 2002.
- [5] Z. Li, J. Sun, and S. Oh, "Design, analysis and experimental validation of a robust nonlinear path following controller for marine surface vessels," *Automatica*, vol. 45, no. 7, pp. 1649–1658, 2009.
- [6] A. Healey and D. Lienard, "Multivariable sliding mode control for autonomous diving and steering of unmanned underwater vehicles," *Oceanic Engineering, IEEE Journal of*, vol. 18, no. 3, pp. 327–339, 1993.
- [7] K. Pettersen and E. Lefeber, "Way-point tracking control of ships," in *Proc. 40th IEEE Conference on Decision and Control*, (Orlando, FL), pp. 940–945, Dec. 2001.
- [8] O. J. Sordalen and O. Egeland, "Exponential stabilization of nonholonomic chained systems," *IEEE Transactions on Automatic Control*, vol. 40, no. 1, pp. 35–49, 1995.
- [9] E. Børhaug and K. Y. Pettersen, "Cross-track control for underactuated autonomous vehicles," in *Proc. 44th IEEE Conference on Decision and Control*, vol. 2005, (Seville, Spain), pp. 602–608, Dec. 2005.
- [10] E. Fredriksen and K. Pettersen, "Global  $\kappa$ -exponential way-point maneuvering of ships: Theory and experiments," *Automatica*, vol. 42, pp. 677–687, Apr. 2006.
- [11] T. I. Fossen and K. Y. Pettersen, "On uniform semiglobal exponential stability (USGES) of proportional line-of-sight guidance laws," *Automatica*, vol. 50, no. 11, pp. 2912–2917, 2014.
- [12] E. Børhaug, A. Pavlov, and K. Y. Pettersen, "Integral LOS control for path following of underactuated marine surface vessels in the presence of constant ocean currents," in *Proc. 47th IEEE Conference on Decision and Control*, (Cancun, Mexico), pp. 4984–4991, 2008.
- [13] W. Caharija, K. Y. Pettersen, M. Bibuli, P. Calado, E. Zereik, J. Braga, J. T. Gravdahl, A. J. Sørensen, M. Milovanović, and G. Bruzzone, "Integral line-of-sight guidance and control of underactuated marine vehicles: Theory, simulations and experiments," *IEEE Transactions on Control Systems Technology*, vol. 24, no. 5, 2016.
- [14] M. S. Wiig, K. Y. Pettersen, and T. R. Krogstad, "Uniform semiglobal exponential stability of integral line-of-sight guidance laws," in *Proc. 10th IFAC Conference on Manoeuvring and Control of Marine Craft*, (Copenhagen, Denmark), pp. 61–68, 2015.
- [15] A. M. Lekkas and T. I. Fossen, "A time-varying lookahead distance guidance law for path following," in *Proc. 9th IFAC Conference on Manoeuvring and Control of Marine Craft*, (Arenzano, Italy), pp. 398–403, 2012.

- [16] A. M. Lekkas and T. I. Fossen, "Minimization of cross-track and along-track errors for path tracking of marine underactuated vehicles," in *Proc. IEEE European Control Conference*, (Strasbourg, France), pp. 3004–3010, 2014.
- [17] A. L. Flåten and E. F. Brekke, "Stability of Line-Of-Sight Based Trajectory-Tracking in Two Dimensions," in *Proc. 1st IEEE Conference on Control Technology and Applications*, (Kohala Coast, HI, USA), pp. 760–765, 2017.
- [18] E. Børhaug, A. Pavlov, E. Panteley, and K. Y. Pettersen, "Straight line path following for formations of underactuated surface vessels," *IEEE Transactions on Control Systems Technology*, vol. 19, no. 3, pp. 493–506, 2011.
- [19] D. J. W. Belleter and K. Y. Pettersen, "Path following for formations of underactuated marine vessels under influence of constant ocean currents," in *Proc. 53th IEEE Conference on Decision and Control*, (Los Angeles, CA, USA), pp. 4521–4528, 2014.
- [20] D. J. W. Belleter and K. Y. Pettersen, "Path following with disturbance rejection for inhomogeneous formations with underactuated agents," in *Proc. IEEE European Control Conference*, (Linz, Austria), pp. 1023–1030, 2015.
- [21] T. I. Fossen, *Handbook of marine craft hydrodynamics and motion control*. John Wiley & Sons, 2011.
- [22] W. Caharija, M. Candeloro, K. Y. Pettersen, and A. J. Sørensen, "Relative velocity control and integral LOS for path following of underactuated surface vessels," in *Proc. 9th IFAC Conference on Manoeuvring and Control of Marine Craft*, vol. 9, pp. 380–385, 2012.
- [23] K. Y. Pettersen, "Lyapunov sufficient conditions for uniform semiglobal exponential stability," *Automatica*, vol. 78, 2017.
- [24] A. Loria and E. Panteley, "Cascaded nonlinear time-varying systems: analysis and design," in *Advanced Topics in Control Systems Theory* (F. Lamnabhi-Lagarigue, A. Loria, and E. Panteley, eds.), ch. 2, pp. 23–64. London: Springer Verlag, 2004.

### APPENDIX I FUNCTIONAL EXPRESSIONS

$$F_{u_r}(v_r, r) \triangleq \frac{1}{m_{11}}(m_{22}v_r + m_{23}r)r \quad (49)$$

$$X(u_r) \triangleq \frac{m_{23}^2 - m_{11}m_{33}}{m_{22}m_{33} - m_{23}^2}u_r + \frac{d_{33}m_{23} - d_{23}m_{33}}{m_{22}m_{33} - m_{23}^2} \quad (50)$$

$$Y(u_r) \triangleq \frac{(m_{22} - m_{11})m_{23}}{m_{22}m_{33} - m_{23}^2}u_r - \frac{d_{22}m_{33} - d_{32}m_{23}}{m_{22}m_{33} - m_{23}^2} \quad (51)$$

$$F_r(u_r, v_r, r) \triangleq \frac{m_{23}d_{22} - m_{22}(d_{32} + (m_{22} - m_{11})u_r)}{m_{22}m_{33} - m_{23}^2}v_r + \frac{m_{23}(d_{23} - m_{11}u_r) - m_{22}(d_{33} + m_{23}u_r)}{m_{22}m_{33} - m_{23}^2}r$$

The functions  $\mathbf{h}_{e_2} \triangleq [h_{e_21}, h_{e_22}, h_{e_23}]^T$  is defined as

$$\begin{aligned} h_{e_21} &= \sin(\tilde{\psi} + \psi_d), \quad h_{e_23} = 0, \\ h_{e_22} &= u_{rd} \left[ \frac{\sin(\tilde{\psi})}{\tilde{\psi}} \cos(\psi_d) + \frac{\cos(\tilde{\psi}) - 1}{\tilde{\psi}} \sin(\psi_d) \right] \\ &+ e_3 \left[ \frac{\cos(\tilde{\psi}) - 1}{\tilde{\psi}} \cos(\psi_d) - \frac{\sin(\tilde{\psi})}{\tilde{\psi}} \sin(\psi_d) \right], \end{aligned} \quad (52)$$

and  $\mathbf{h}_{e_3} \triangleq [h_{e_31}, h_{e_32}, h_{e_33}]^T$  is

$$\begin{aligned} h_{e_31} &= \frac{X(\tilde{u}_r + u_{rd}) - X^{u_{rd}}}{\tilde{u}_r} k_{\Delta} \gamma(e_1, e_2, e_3) \\ &+ e_3 \frac{Y(\tilde{u}_r + u_{rd}) - Y^{u_{rd}}}{\tilde{u}_r}, \\ h_{e_32} &= 0, \quad h_{e_33} = X(\tilde{u}_r + u_{rd}). \end{aligned} \quad (53)$$

The limits of  $h_{e_22}$  for  $\tilde{\psi} \rightarrow 0$  and  $h_{e_31}$  as  $\tilde{u}_r \rightarrow 0$  exist and are finite. The expression  $\gamma(e_1, e_2, e_3)$  used in  $h_{e_31}$  is defined as

$$\begin{aligned} \gamma(e_1, e_2, e_3) &\triangleq u_{rd}^2 \frac{(e_2 + \sigma y_{\text{int}}^{\text{eq}}) - k_{\Delta} e_3}{h(e_2)^{3/2}} - \frac{u_{rd} V_y}{h(e_2)} \\ &- \frac{\sigma k_{\Delta} u_{rd}^2}{h(e_2)^2} (e_2 - e_1 \sigma) + \frac{\tilde{u}_{rd} (\sigma y_{\text{int}}^{\text{eq}} + e_2)}{h(e_2)} \end{aligned} \quad (54)$$